Contributions to Geophysics and Geodesy Vol. 53/4, 2023 (333–351)

1D along-track pre-processing of the GOCE gravity gradients and nonlinear filtering of the radial components V_{zz} in spatial domain

Róbert ČUNDERLÍK*, Michal KOLLÁR, Karol MIKULA

Department of Mathematics and Descriptive Geometry, Faculty of Civil Engineering, Slovak University of Technology, Radlinského 11, 810 05 Bratislava, Slovak Republic

Abstract: The paper presents pre-processing and nonlinear filtering of the GOCE gravity gradients (GGs) in spatial domain. At first, a multiple fully automatic 1D along-track pre-processing of the GOCE GGs in the gradiometer reference frame (GRF) is introduced. This tool is based on the nonlinear diffusion filtering in 1D while treating issues like a detection of 'jumps' in time series, outliers and unforeseen systematic tendencies. We focus on the 1D along-track pre-processing of the GOCE GGs in GRF for the last period of the GOCE satellite mission (from 2012-12-01 to 2013-10-19) that are later transformed into the local north-oriented frame (LNOF). Afterwards, the radial components V_{zz} are reduced on a reference surface chosen as a mean value of all altitudes of the GOCE satellite orbits from the processed period. Here they are filtered using the nonlinear diffusion filtering on a closed surface. Finally, a grid of the filtered radial components V_{zz} in LNOF on the reference surface is obtained.

Key words: GOCE gravity gradients, 1D along-track pre-processing, jump detection, nonlinear diffusion filtering, grid of the filtered radial components V_{zz} in LNOF

1. Introduction

In this paper we summarize main results achieved within the ESA PECS project "GOCE-based high-resolution gravity field modelling in a space domain (GOCE-numerics)" (see Acknowledgment), namely of its first phase devoted to processing and filtering of the GOCE gravity gradients (GGs). In this project we developed a tool for automatic 1D along-track pre-processing of the GOCE GGs in the gradiometer reference frame (GRF). Section 2 describes details and mathematical background of our approach designed for this tool while treating issues like a detection of 'jumps' in time series, outliers and unforeseen systematic tendencies.

*corresponding author, e-mail: robert.cunderlik@stuba.sk

doi: 10.31577/congeo.2023.53.4.2

As input data we have used the EGG_NOM_2 product provided by ESA (*ESA, 2014*) while the GOCE GGs have been corrected from perturbations caused by the geomagnetic field (*Siemes, 2018*). Due to a measurement band of the gradiometer, such GGs contain valuable information about the Earth's gravity field in the corresponding bandwidth, however, the low-frequency part of the signal is not detected accurately. Consequently, the values of GGs in the EGG_NOM_2 product do not represent 'realistic' values (*Bouman et al., 2011*). In the case of filtering such data in the spatial domain as proposed in this project, this drawback should be overcome.

Section 3 presents results of the 1D along-track pre-processing of the GOCE GGs in GRF for the last period of the GOCE satellite mission, namely from 2012-12-01 to 2013-10-19. Here the GOCE GGs are pre-processed by removing a low-frequency part of the gravity field generated from a chosen GRACE/GOCE-based model, i.e. by removing spherical harmonics (SH) up to d/o 10. Afterwards, such pre-processed GOCE GGs in GRF are transformed into the local north-oriented frame (LNOF). Section 4 is dealing with the nonlinear diffusion filtering of the radial components V_{zz} considered on a reference surface, which represents a mean value of all altitudes of the GOCE observations from the processed period. Finally, a grid of the filtered components V_{zz} in LNOF on the reference surface is obtained. Conclusions in Section 5 summarized our results.

2. 1D along-track pre-processing of the GOCE GGs in GRF

In this section, we present multiple fully automatic pre-processing methods we have designed in order to process and filter the GOCE GGs. To treat the problem in spatial domain, we have evaluated residuals between the GOCE GGs in GRF and GGs generated from the official SH-based model provided by ESA, namely from the GO_CONS_GCF_2_TIM_R5 model up to d/o 280 (*Brockmann et al., 2014*). These residuals represent time series as our input data for processing, however, they are apparently affected by unforeseen biases and trends. In all time series we can see large biases for different components as well as numerous 'jumps', some of them small but some of them reaching large values. Hence, the developed tool has been designed to overcome these issues.

The first part describes a mathematical background of the linear and nonlinear diffusion for processing 1D time series that have been proposed to process the GOCE GGs. The second part is dedicated to a 'jump' detection using the developed nonlinear diffusion. The third part presents an approach how to remove unforeseen trends from the processed time series. For an illustration of input data, we choose the time series from 2010-10-01 00:00:00 to 2010-10-04 22:10:22. Figure 1 depicts residuals in this period for the components $\mathrm{d}V_{xx}$, $\mathrm{d}V_{yy}$, $\mathrm{d}V_{zz}$ and $\mathrm{d}V_{xz}$. Two others components $\mathrm{d}V_{xy}$ and $\mathrm{d}V_{yz}$ are not considered since they are less accurately observed (*Bouman et al., 2011*).

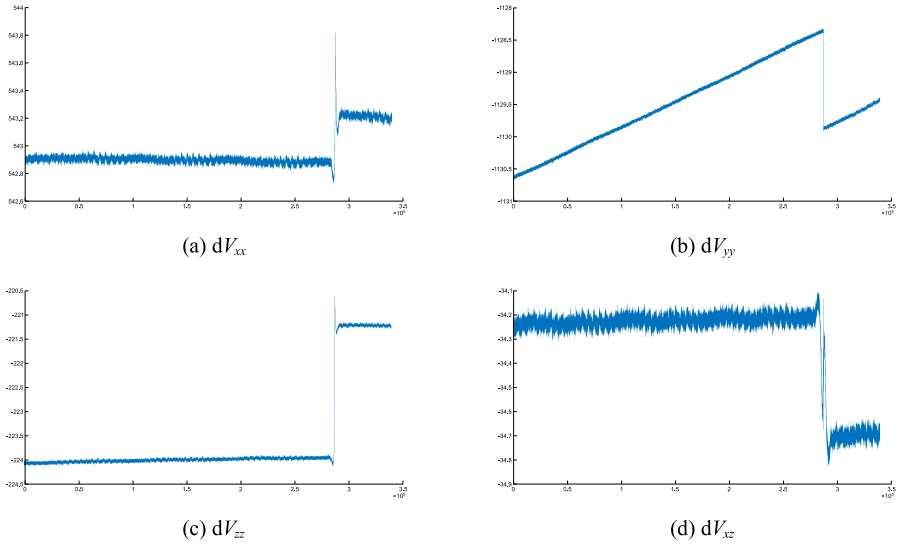

(a) $\mathrm{d}V_{xx}$ (b) $\mathrm{d}V_{yy}$

(c) $\mathrm{d}V_{zz}$ (d) $\mathrm{d}V_{xz}$

Fig. 1. Residuals between the GOCE GGs in GRF and GGs generated from the GO_CONS_GCF_2_TIM_R5 model up to d/o 280 (period: 2010-10-01 00:00:00 – 2010-10-04 22:10:22, units: E).

2.1. The linear and nonlinear diffusion for processing 1D time series

A simple differential equation in the form:

$$u_t = u_{xx} \tag{1}$$

represents a linear diffusion of 1D time series. The values $u(x,t)$ represent the processed data while $u(x,0)$ is an initial condition for Eq. (1) given

by the original time series. Let us remark that t in Eq. (1) represents an artificial 'filtering' time and x represents the original time coordinates of the time series which we process. Using the backward difference to approximate the time derivative u_t and the central second difference to approximate the second spatial derivative u_{xx}, we get the Eq. (1) in the form:

$$\frac{u_i^j - u_i^{j-1}}{\tau} = \frac{u_{i-1}^j - 2u_i^j + u_{i+1}^j}{h^2}\,, \tag{2}$$

where $\tau = t_j - t_{j-1}$ denotes the time step, h denotes spatial step and the value of u_i^j represents a solution in the j^{th} time (filtering) step and at i^{th}, $i = 1, ..., N$, point of the time series. After simple manipulation in the equation, we get an implicit numerical scheme for 1D linear diffusion in the form:

$$-\frac{\tau}{h^2}\, u_{i-1}^j + \left(1 + \frac{2\tau}{h^2}\right) u_i^j - \frac{\tau}{h^2}\, u_{i+1}^j = u_i^{j-1}\,. \tag{3}$$

For $i = 1, ..., N$, these equations represent a system of linear equations $Au^j = u^{j-1}$, for solution at j^{th} time step, where A is a three-diagonal matrix with coefficients $a_{i,i-1} = a_{i,i+1} = -\frac{\tau}{h^2}$ and $a_{i,i} = 1 + \frac{2\tau}{h^2}$ in i^{th} row of the matrix. In the case of implicit numerical scheme, the scheme is stable for any selection of τ. As boundary conditions, we use the Dirichlet conditions $u_0^j = u_0^0$ and $u_N^j = u_N^0$.

For the 1D nonlinear diffusion of a time series, we use the Perona-Malik diffusion equation (*Perona and Malik, 1987*) in the form:

$$u_t = \left(g\left(|u_x^\sigma|\right) u_x\right)_x\,. \tag{4}$$

In this case, the diffusion is affected by the nonlinear function $g\left(|u_x^\sigma|\right)$, which represents an edge detection function (or in the meaning of our data – 'jump' detection function). The detector function is defined as:

$$g\left(|u_x^\sigma|\right) = \frac{1}{1 + K|u_x^\sigma|^2}\,, \tag{5}$$

where u_x^σ represent derivative (1D-gradient) of the solution obtained by the linear diffusion with the timestep σ and K is a sensitivity parameter. This equation is numerically solved by the finite difference method. After applying the finite difference to Eq. (4) we get the equation in the form:

$$\frac{u_i^j - u_i^{j-1}}{\tau} = \frac{1}{h}\left(g\left(\left|u_x^{j-1,\sigma}\right|_{i+\frac{1}{2}}\right)\frac{u_{i+1}^j - u_i^j}{h} - g\left(\left|u_x^{j-1,\sigma}\right|_{i-\frac{1}{2}}\right)\frac{u_i^j - u_{i-1}^j}{h}\right), \quad (6)$$

where:

$$\left|u_x^{j-1,\sigma}\right|_{i+\frac{1}{2}} = \left|u_{i+1}^{j-1,\sigma} - u_i^{j-1,\sigma}\right|/h \quad \text{and} \quad \left|u_x^{j-1,\sigma}\right|_{i-\frac{1}{2}} = \left|u_i^{j-1,\sigma} - u_{i-1}^{j-1,\sigma}\right|/h\,.$$

We will denote $g\left(\left|u_x^{j-1,\sigma}\right|_{i+\frac{1}{2}}\right)$ as $g_{i+\frac{1}{2}}^{j-1,\sigma}$ and $g\left(\left|u_x^{j-1,\sigma}\right|_{i-\frac{1}{2}}\right)$ as $g_{i-\frac{1}{2}}^{j-1,\sigma}$. Subsequently, after simple manipulations, we can express the final semi-implicit numerical scheme for 1D nonlinear diffusion in the form:

$$-\frac{\tau}{h^2}\,g_{i-\frac{1}{2}}^{j-1,\sigma}u_{i-1}^j + \left[1 + \frac{\tau}{h^2}\left(g_{i-\frac{1}{2}}^{j-1,\sigma} + g_{i+\frac{1}{2}}^{j-1,\sigma}\right)\right]u_i^j - \frac{\tau}{h^2}\,g_{i+\frac{1}{2}}^{j-1,\sigma}u_{i+1}^j = u_i^{j-1}. \quad (7)$$

The system matrix A of the system of linear equations $Au^j = u^{j-1}$ is again given by the three-diagonal matrix with the coefficients:

$$a_{i,i-1} = -\frac{\tau}{h^2}\,g_{i-\frac{1}{2}}^{j-1,\sigma},\ a_{i,i+1} = -\frac{\tau}{h^2}\,g_{i+\frac{1}{2}}^{j-1,\sigma} \quad \text{and}$$

$$a_{i,i} = 1 + \frac{\tau}{h^2}\left(g_{i-\frac{1}{2}}^{j-1,\sigma} + g_{i+\frac{1}{2}}^{j-1,\sigma}\right),\ i = 1, ..., N\,.$$

This semi-implicit scheme is stable for any selection of τ. As boundary conditions, we use the Dirichlet boundary conditions $u_0^j = u_0^0$ and $u_N^j = u_N^0$.

2.2. 'Jump' detection

For the 'jump' detection we utilize a behaviour of the nonlinear Perona-Malik diffusion applied to the time series. A main idea of this approach is the fact that the nonlinear Perona-Malik diffusion significantly smooths time series while preserves areas with high gradients (*Perona and Malik, 1987*) – i.e. also areas of 'jumps'. After one large step of the nonlinear diffusion, we evaluate gradients of the solution. If those gradients yield high values (value is larger than the specific threshold value δ), there is a 'jump' in time series. In our 'jump' detection approach we use parameters for the nonlinear diffusion as $\sigma = 5000$, $\tau = 120000$, $K = 10^{11}$ and as a threshold value we use $\delta = 10^{-6}$. These parameters were tuned experimentally such that the 'jump' detection results are in an agreement with results of the

visual inspection performed on several testing datasets. Afterwards, based on a location of the value u_i with large gradient, we applied a $mask$ on the neighbouring locations $k, k \in (i - 1000, i + 1000)$ as $mask(u_k) = 0$ (note that the number of points with an applied $mask$ before and after the 'jump' is approximately half of the number of points on each ascending or descending track). Outside this interval we use $mask(u_i) = 1$. After estimation of parameters we can automatically detect and mark all significant 'jump' areas in data.

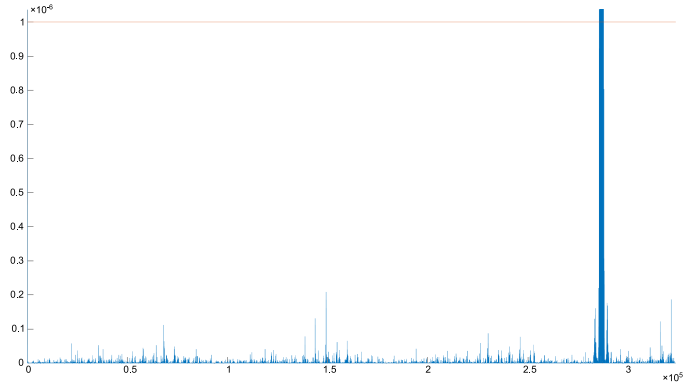

(a) Gradients evaluated from $\mathrm{d}V_{xx}$

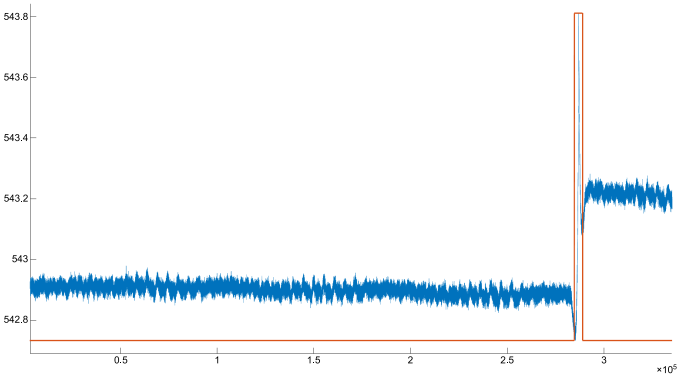

(b) Mask over $\mathrm{d}V_{xx}$

Fig. 2. (a) Values of evaluated gradients (blue) with the specified threshold (orange line) and (b) corresponding residuals (blue) with 'jump' mask (orange) (for visualization purposes the mask is scaled to minimal a maximal value of time series; units: E).

Subsequently, we split the time series into tracks and in each ascending and descending track, we check a value of the defined $mask$. If any point of the track yields $mask(u_i) = 0$, we replaced each u_i in that track by value obtained by a linear interpolation. Boundary values for the linear interpolation are given by values in boundary nodes obtained from the solution of the nonlinear Perona-Malik diffusion, which we used for the 'jump' detection. After this replacement, we get modified 'clean' times series without any significant 'jumps' in data. Figure 2a depicts values of gradients from the solution of nonlinear diffusion of $\mathrm{d}V_{xx}$ component with the threshold $\delta = 10^{-6}$ while Figure 2b depicts the residuals of $\mathrm{d}V_{xx}$ with a generated mask. Other examples of detailed segments from the 'jump' areas of pre-processed time series are depicted in Figure 3. In this figure, the blue time series represent original residuals and the orange time series represent 'clean' data without 'jumps'. This data are used as an input of our next step in data pre-processing – a trend detection and elimination.

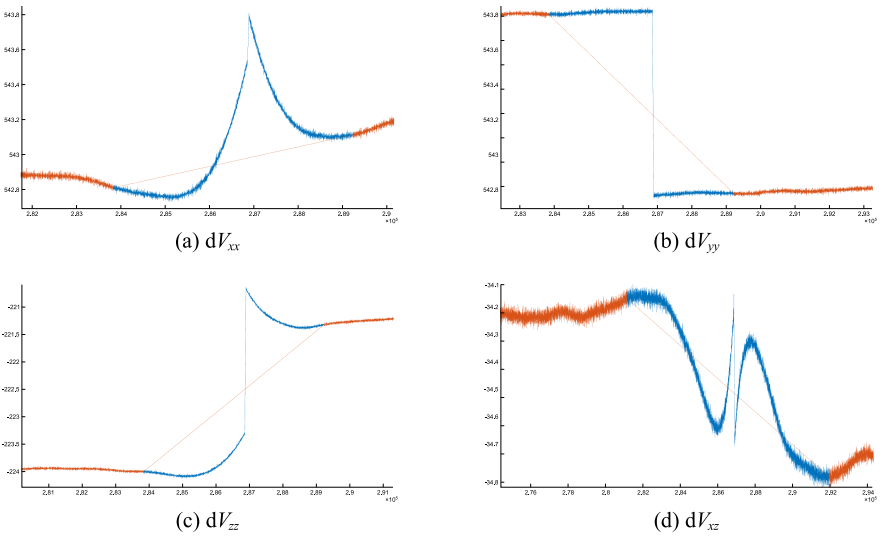

Fig. 3. Detailed segments from original residuals (blue) and residuals with removed 'jumps' (orange) (units: E).

2.3. Trend detection and its elimination

Besides detected jumps and biases, one can see some periodicity in the different time series with changing amplitudes (Fig. 4). To analyse such data,

at first we have fitted the residuals by a constant value separately for each ascending and descending track. Surprisingly, the residuals include some trends or 'systematic tendencies' which look different for the ascending and descending tracks. They have different behaviour for every GGs component but in all cases they have a long-wavelength character with amplitudes reaching several mE.

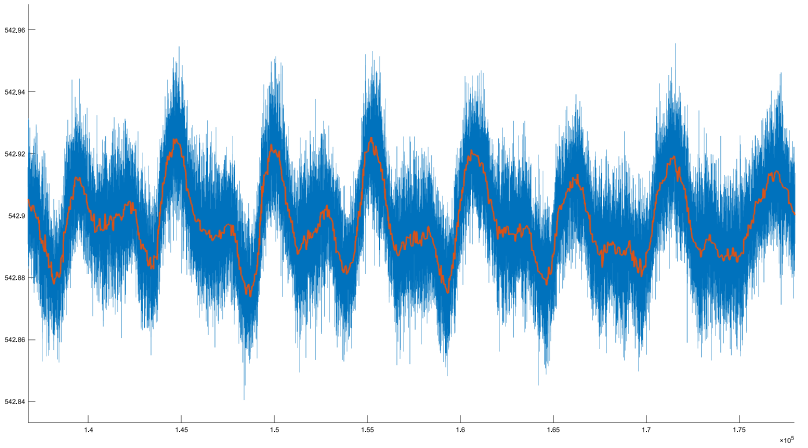

Fig. 4. Residuals dV_{xx} – a detail of the time series in Fig. 2b after 'jump' detection process (in blue) and the optimal solution of the nonlinear diffusion based on the Perona-Malik model (in orange) (units: E).

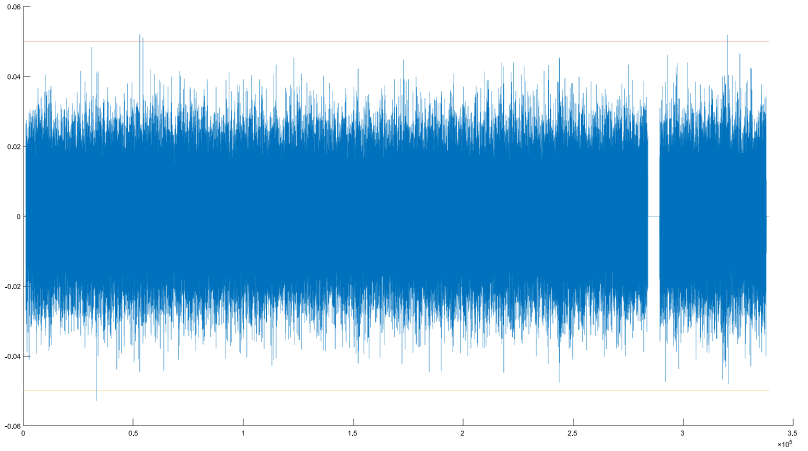

Fig. 5. *Residuals* dV_{xx} – corrected time series from Fig. 1a without 'jumps' and trends (units: E).

Figure 6 shows such residuals after fitting by a constant for different components of the GOCE GGs observed during the last 2.5 months of the GOCE satellite mission. Apparently, the trends or 'systematic tendencies' of several mE dominate in the signal. Moreover, they are slightly changing in

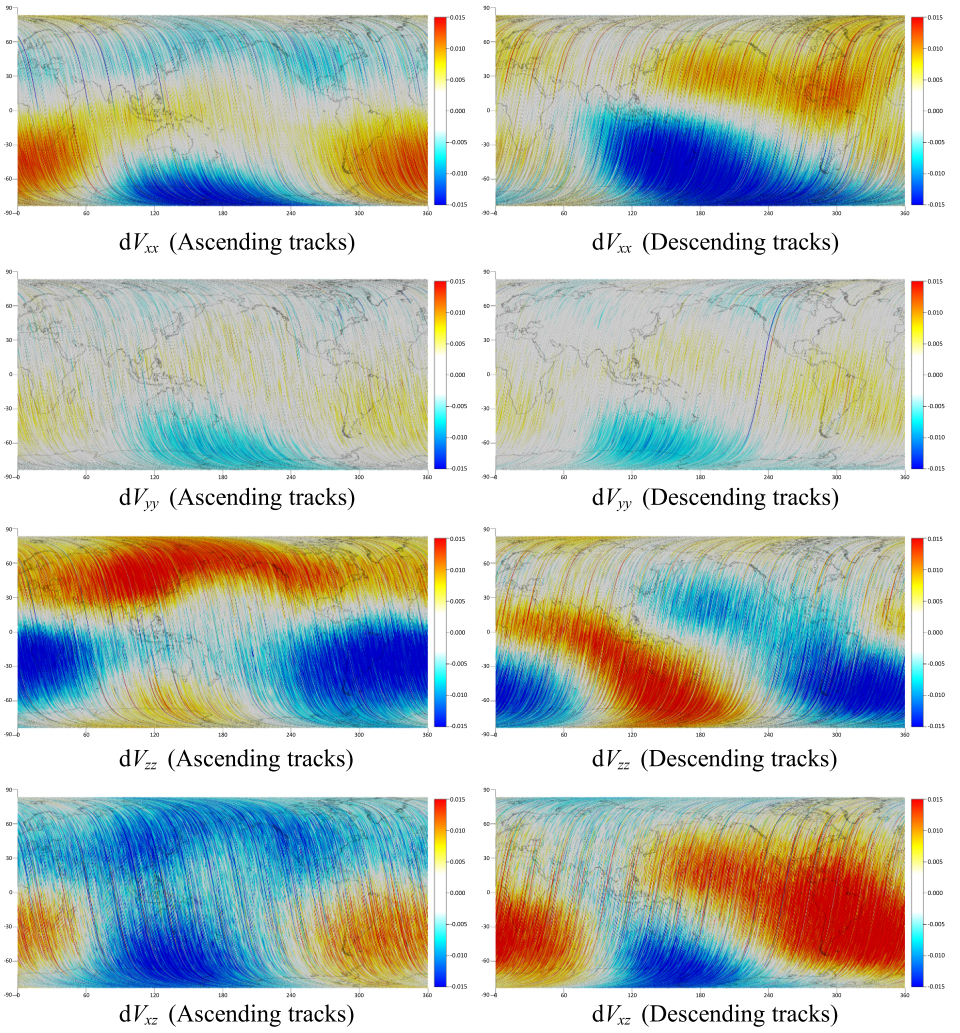

Fig. 6. The 'systematic tendencies' of the GOCE GGs in GRF depicted in the geolocated spatial domain after removing a constant bias separately for each ascending and descending track (Period: 2013-08-04 – 2013-10-19, units: E).

time when depicted for different 2-months periods. As we know, these trends usually vanish when processing the GOCE observations in spectral domain because the GGs are treated only for the measurement bandwidth of the gradiometer (*Bouman et al., 2011*). Due to their low-frequency character, they are thus removed together with the low-frequency signal of the GOCE measurements, which is not detected accurately.

In the case of processing the GOCE GGs in spatial domain, we have to remove these unforeseen 'systematic tendencies'. Therefore, we have decided to model and remove them as unforeseen trends directly from the time series. For this purpose, we have again used the 1D Perona-Malik diffusion equation (4). On the contrary to the 'jump' detection approach, now we have used several steps of nonlinear diffusion with different timesteps. The number of steps and size of timesteps has been influenced by a prescribed stopping criterion. The design of this criterion has been based on behaviour of the variation of a total number of extremal values during the diffusion process. In general, if the difference between number of extremal values in two consecutive steps is small enough, we can say, that the current solution contains only the solicited trend. Extremal values are given by values u_i which fulfil conditions $u_i^j < u_{i-1}^j$ and $u_i^j < u_{i+1}^j$, or, $u_i^j > u_{i-1}^j$ and $u_i^j > u_{i+1}^j$. In our pre-processing we have used a stopping criterion as a condition which is satisfied if the difference between number of extremal values is smaller than 50. Figure 5 depicts new corrected time series after removing the trends.

3. Pre-processing of the GOCE GGs in GRF by removing low frequencies up to d/o 10

In the previous section, we have presented pre-processing of the residuals between the GOCE GGs in GRF from the SGG_NOM_2 product and the full spectrum (SH up to d/o 280) of the GO_CONS_GCF_2_TIM_R5 model. However, to better reflect the geophysical signal detected by the GOCE mission, we have again pre-processed the GOCE GGs by removing only a low-frequency part (SH up to d/o 10) generated from the GRACE/GOCE-based model, namely from the GO_CONS_GCF_2_DIR_R5 (*Bruinsma et al., 2013*). Hence, we have again applied the developed 1D along-track nonlinear pre-processing to new residuals that contain more geophysical

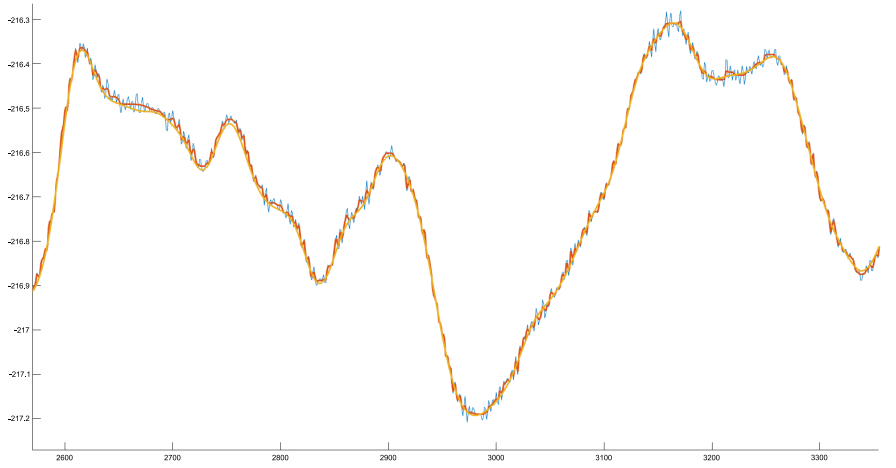

Fig. 7. 1D along-track pre-processing of the GOCE GGs in GRF (component V_{zz}); residuals after removing the GO_CONS_GCF_2_DIR_R5 up to d/o 10 (blue line), filtered data using the Perona-Malik model (red line), and the GO_CONS_GCF_2_DIR_R5 (SH between d/o 10 and 300) shifted by a constant (orange line) (units: E).

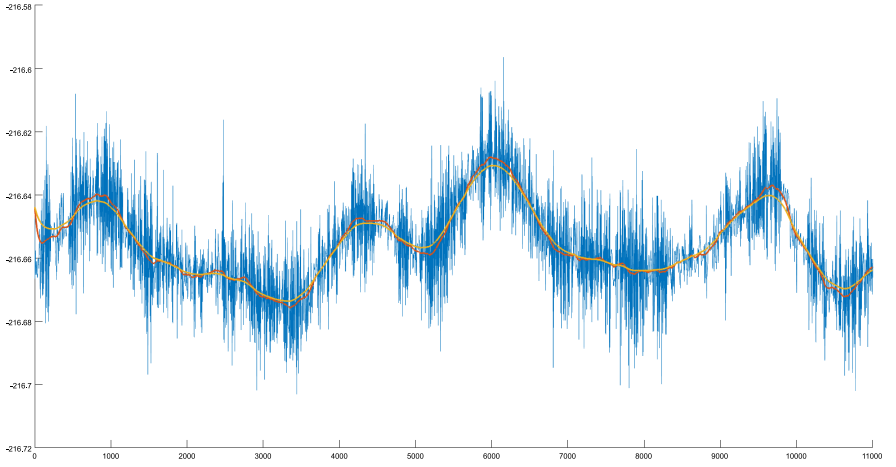

Fig. 8. Comparison of the filtered GOCE GGs (component V_{zz}) with the GO_CONS_GCF_2_DIR_R5 using SH between d/o 10 and 300 (blue line), and its 1D along-track linear filtering after 300 steps (red line) and 20000 steps (orange line) of the linear diffusion (units: E).

signal. Figure 7 depicts an example of such residuals after removing the GO_CONS_GCF_2_DIR_R5 up to d/o 10 (blue line), our filtered data using the Perona-Malik model (red line) and the GO_CONS_GCF_2_DIR_R5 (SH between d/o 10 and 300) shifted by a constant value (orange line).

The crucial step of such pre-processing is to fit the residuals to 'correct values', i.e. to eliminate extreme biases. For these purposes we have used the rest frequencies of the GO_CONS_GCF_2_DIR_R5 spectrum, i.e. SH between 10 and 300. However, its comparison with the filtered residuals have shown significant periodicities correlated with the GOCE orbit cycles (Fig. 8, blue lines). These periodicities are again different for each component of the GOCE GGs and they are different for the ascending and descending tracks. In geolocated spatial domain they look similar as the 'systematic tendencies' that have been presented and discussed in the previous section (Fig. 6).

To remove these periodicities, we have again applied the 1D along-track linear filtering (Section 2.3). However, such linear filtering has step-by-step smoothed local extremes (compare the red and orange lines in Fig. 8). Consequently, this has yielded a remaining part of the 'systematic tendencies'. When depicting the residuals of the filtered component dV_{zz} and values generated from the GO_CONS_GCF_2_DIR_R5 (SH between d/o 10 and 300)

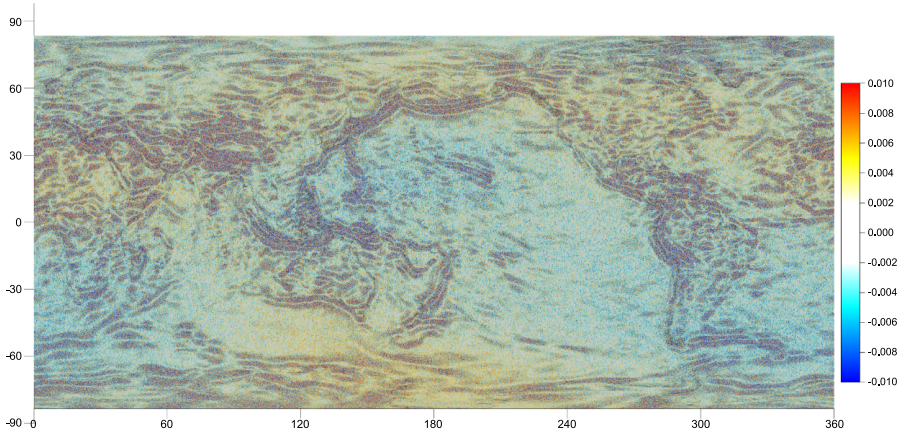

Fig. 9. Residuals between the filtered GOCE GGs (component V_{zz}) using the 1D along-track pre-processing and the GO_CONS_GCF_2_DIR_R5 considering SH between d/o 10 and 300 (units: E).

in geolocated spatial domain, there is an evident trend remaining in such residuals (Fig. 9). Therefore, we have had to model this remaining trend and remove it from data. For this purpose, we have used the linear diffusion filtering of the residuals on closed surfaces (*Čunderlík et al., 2013, 2016*). Figure 10 depicts the determined trend that has been removed from the filtered GOCE GGs. Figure 11 shows residuals of the corrected radial

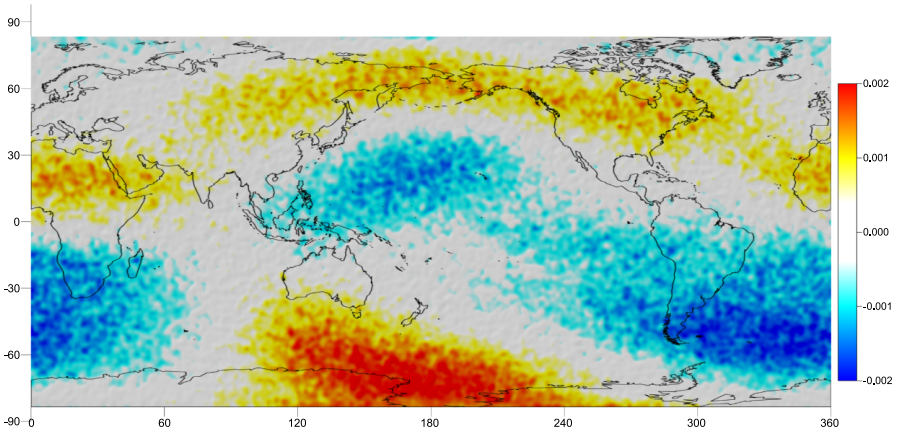

Fig. 10. The trend detected from the residuals in Fig. 9 using the linear diffusion filtering (units: E).

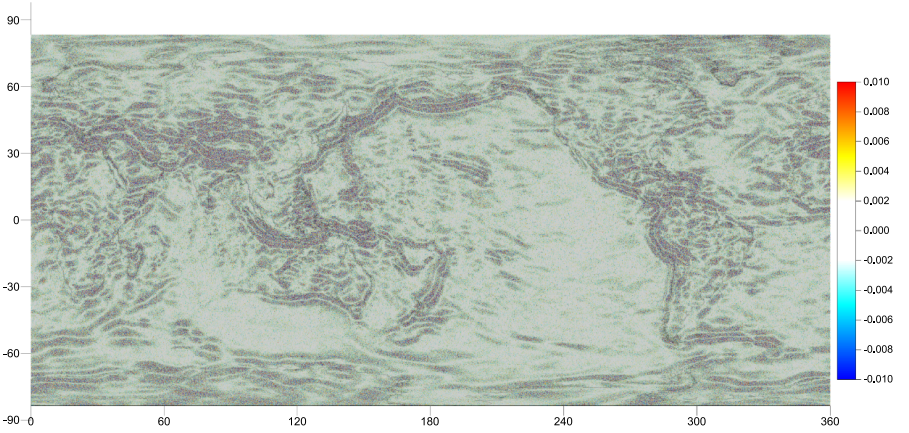

Fig. 11. Residuals between the filtered GOCE GGs (component V_{zz}) after removing the trend and the GO_CONS_GCF_2_DIR_R5 considering SH between d/o 10 and 300 (units: E).

components dV_{zz} with respect to the GO_CONS_GCF_2_DIR_R5 (SH between d/o 10 and 300). Remark: due to the fact that this trend is slightly changing in time, we have modelled the trends separately for each dataset of 61 days of the GOCE measurements.

4. Nonlinear filtering of the radial components V_{zz} in LNOF on a mean reference surface

Afterwards, the pre-processed GOCE GGs with removed trends have been transformed from the GRF into LNOF. In this process, two less precise components V_{XY} and V_{YZ} have been replaced by values generated from the GO_CONS_GCF_2_TIM_R5 model up to d/o 280. Consequently, the transformed components in LNOF have strong dependencies on this model (*Bouman et al., 2011*). The smallest dependency about few % is in the case of the radial component V_{zz}. Therefore, in the following we have focused on further processing and filtering only the radial component V_{zz}.

Our aim had been to create a grid of the filtered components V_{zz}. Due to different altitudes of the original GOCE measurements (Fig. 12), we have decided to relate the grid values to some reference surface. Taking into account that the GOCE satellite mission detected more geophysical signal after lowering its orbit, we decided to process observations from the last period of the GOCE mission, namely from the period between 2012-12-01 and 2013-10-19. The reference surface has been defined as a mean value of altitudes of the GOCE satellite orbits from its last 4-months period. The graph on Figure 12 shows mean altitudes of the GOCE orbits during its whole observing period while our mean reference surface has been chosen at altitude of 240 km (depicted by the red line).

In reality, altitudes of the ascending and descending tracks could vary several km above the same geolocated place. Moreover, altitudes above the southern polar regions were more than 15 km higher as those above the northern polar regions (Fig. 13 left). Therefore, the reference surface was designed as a mean value of altitudes (Fig. 13 right) and it was obtained by the linear diffusion filtering of all altitudes of the GOCE observations from the period between 06/2013 and 10/2013 (Fig. 12).

To reduce an impact of different altitudes on the observed GOCE GGs, we have evaluated corrections from heights using the values generated from

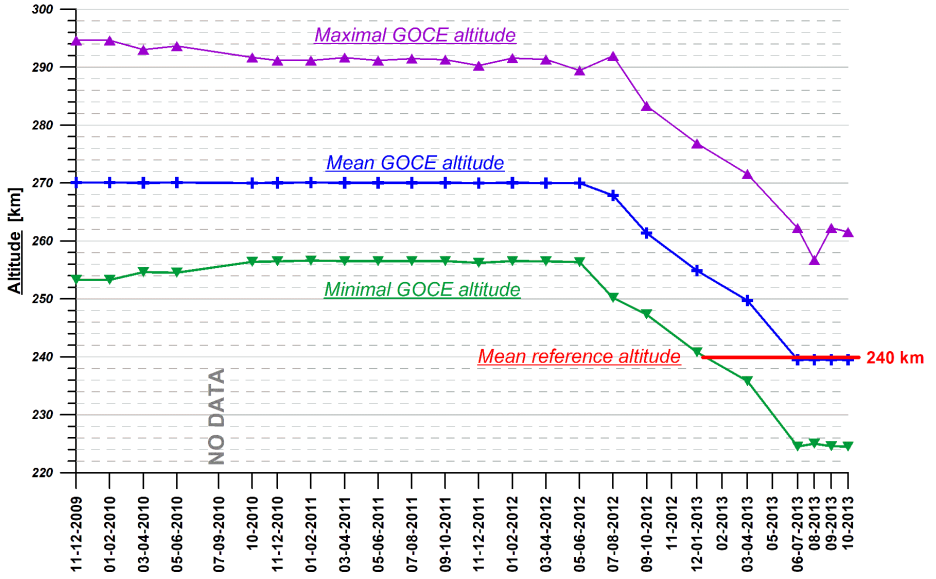

Fig. 12. Altitudes of the GOCE satellite orbits during its whole observing period and the chosen mean reference altitude for nonlinear filtering of the V_{zz} component.

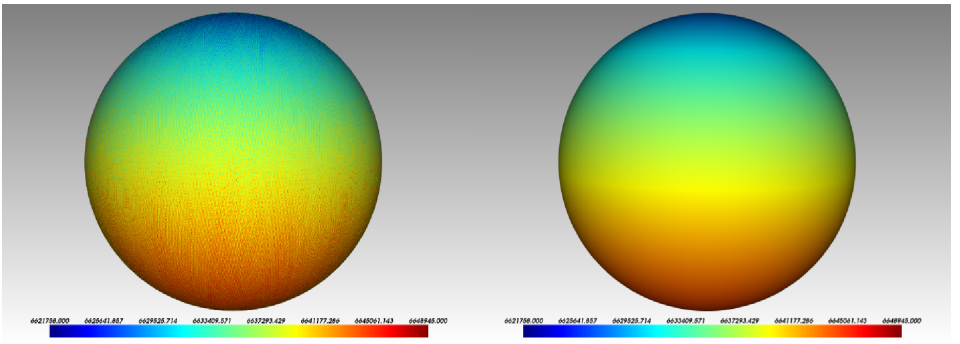

Fig. 13. The GOCE satellite orbits during the period: 06/2013 – 10/2013 (left), and the reference surface as a mean value obtained by the linear diffusion filtering (right), (radial distances from the geocenter in meters).

the GO_CONS_GCF_2_TIM_R5 up to d/o 280. Although this approach could involve a slight dependence on this model, such corrections have been evaluated more precisely as to use the original GOCE measurements affected by noise. According to our experiences, amplitudes of the noise have

been often higher than the evaluated corrections. Considering the modelled corrections from heights, we have finally got the radial components $\mathrm{d}V_{zz}$ in the LNOF obtained on the reference surface, see Fig. 14 (above).

Apparently, such pre-processed data are still very noisy. To reduce the noise, we have applied nonlinear diffusion filtering on closed surfaces using the Perona-Malik model (*Čunderlík et al., 2016*). Figure 14 (below) shows the filtered components $\mathrm{d}V_{zz}$ in the LNOF. After restoring the low frequen-

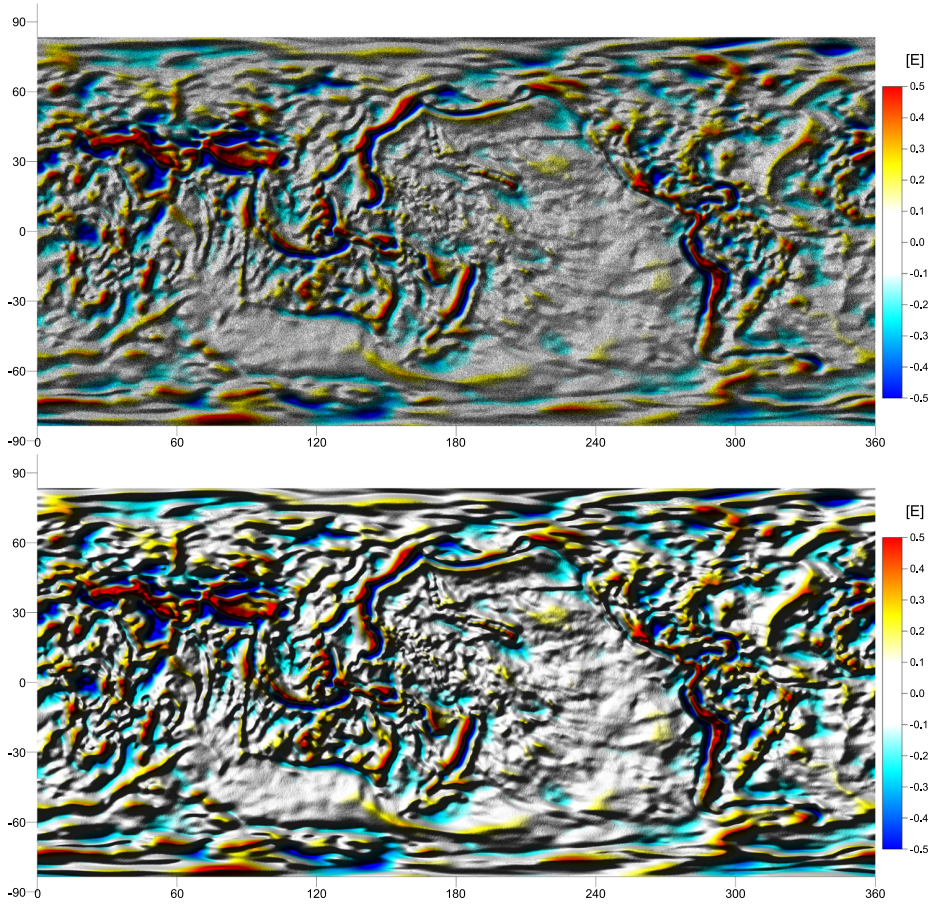

Fig. 14. Pre-processed GOCE GGs in the LNOF (component V_{zz}) using the 1D along-track pre-processing after removing the GO_CONS_GCF_2_DIR_R5 up to d/o 10 (above); and their filtered values after nonlinear diffusion filtering on closed surfaces (below). Processed data are from the period: 2012-12-01 – 2013-10-19.

cies from the GO_CONS_GCF_2_DIR_R5 up to d/o 10, we have got a final grid of the filtered GOCE GGs in the LNOF, namely the radial components V_{zz} obtained on the mean reference surface (Fig. 13 right).

Finally, Figure 15 depicts residuals between the obtained radial components V_{zz} in LNOF and values generated from the GO_CONS_GCF_2_TIM_R5 up to d/o 280. It is evident that some noise has remained, however, now it is much smaller (compare Fig. 15 and Fig. 11). Strong noise reaching amplitudes more than ± 10 mE, which remained in the areas of higher gradients in geophysical signal after pre-processing in GRF (Fig. 11), has been reduced significantly. After the nonlinear filtering, the residuals in Figure 15 are in the range of ± 3 mE. Apart from an evident pattern along the magnetic equator, they look more like a noise. However, when achieving such accuracy, it is difficult to say what is noise and what is signal. Therefore, we have stopped the nonlinear filtering in this stage to avoid further smoothing of the geophysical signal.

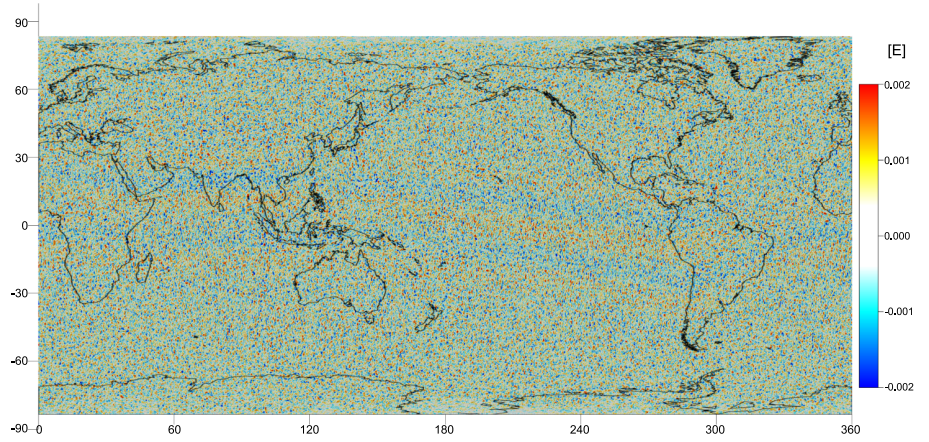

Fig. 15. Residuals between the pre-processed and filtered GOCE GGs in the LNOF (component V_{zz}) and the GO_CONS_GCF_2_TIM_R5 up to d/o 280. Processed data are from the period: 2012-12-01 – 2013-10-19.

5. Summary and conclusions

In Section 2 we have introduced the fully automatic 1D along-track preprocessing of the GOCE GGs in GRF. This tool based on the nonlinear diffusion filtering in 1D using the Perona-Malik model has proved to be effi-

cient for processing the GOCE GGs provided by the EGG_NOM_2 product (*ESA, 2014*). It has allowed us to reduce high biases while treating the issues like a detection of 'jumps' in time series, outliers or unforeseen systematic tendencies. Our pre-processing has shown that these unforeseen systematic tendencies have a long-wavelength character reaching almost ± 20 mE and they look different for every GGs component (Fig. 6). Moreover, they are slightly changing in time when depicted for different 2-months periods. This could be of interest for further investigations. Nevertheless, when processing the GOCE GGs in spectral domain, these systematic tendencies usually vanish, because only the measurement bandwidth of the gradiometer is considered.

In the second part we have focused on pre-processing and filtering of the GOCE GGs for the last period of the GOCE satellite mission, namely from 2012-12-01 to 2013-10-19. For the 1D along-track pre-processing of the GGs in GRF, the low-frequency part of the gravity field generated from the GO_CONS_GCF_2_DIR_R5 up to d/o 10 has been removed. Here the remained signal of the unforeseen systematic tendencies reaching about ± 2 mE has to be modelled and removed. Afterwards, the pre-processed GOCE GGs in GRF could be transformed into LNOF. However, replacing of two less precise components V_{xy} and V_{yz} by values generated from the GO_CONS_GCF_2_TIM_R5 has caused strong dependencies on this model. Therefore, we have focused solely on the radial component V_{zz}, in which such a dependency is only few % (*Bouman et al., 2011*).

Finally, the radial components V_{zz} in LNOF have been filtered on the reference surface using the nonlinear diffusion filtering. The reference surface has been chosen as a mean value of all altitudes of the GOCE satellite orbits from the processed period (Fig. 13). In this way we have aimed to get the filtered GOCE GGs closer to altitudes of the real GOCE measurements than to evaluate them on a surface with constant ellipsoidal heights. Hence, an impact of the corrections from heights has been minimized.

Our main result is the grid of the filtered radial components V_{zz} in LNOF on the reference surface. Their comparison with the values generated from of the GO_CONS_GCF_2_TIM_R5 up to d/o 280 (Fig. 15) shows that our data are noisier, however, the residuals in the range of ± 3 mE indicate high accuracy of the obtained radial components V_{zz} in LNOF. The same procedure can be also applied for other components of the GOCE GGs in LNOF,

however, an aforementioned impact of the modelled components V_{xy} and V_{yz} will be much higher. Anyhow, the obtained grid of the filtered radial components V_{zz} in LNOF can be used for static global gravity field modelling or further analysing the geophysical signal detected by the GOCE satellite mission.

Acknowledgements. Funded by the Government of Slovakia through an ESA Contract under the PECS (Plan for European Cooperating States), namely through the PECS contract SK2-08: "GOCE-based high-resolution gravity field modelling in a space domain (GOCE-numerics)". The view expressed herein can in no way be taken to reflect the official opinion of the European Space Agency. This work was also supported by the Grants VEGA 1/0486/20 and APVV-19-0460.

References

Bouman J., Fiorot S., Fuchs M., Gruber T., Schrama E., Tscherning C., Veicherts M., Visser P., 2011: GOCE gravitational gradients along the orbit. J. Geod., **85**, 11, 791–805, doi: 10.1007/s00190-011-0464-0.

Brockmann J. M., Zehentner N., Höck E., Pail R., Loth I., Mayer-Gürr T., Schuh W.-D., 2014: EGM_TIM_RL05: An independent geoid with centimeter accuracy purely based on the GOCE mission. Geophys. Res. Lett., **41**, 22, 8089–8099, doi: 10.1002/2014GL061904.

Bruinsma S. L., Förste C., Abrikosov O., Marty J.-C., Rio M.-H., Mulet S., Bonvalot S., 2013: The new ESA satellite-only gravity field model via the direct approach. Geophys. Res. Lett., **40**, 14, 3607–3612, doi: 10.1002/grl.50716.

Čunderlík R., Kollár M., Mikula K., 2016: Filters for geodesy data based on linear and nonlinear diffusion. Int. J. Geomath., **7**, 2, 239–274, doi: 10.1007/s13137-016-0087-y.

Čunderlík R., Mikula K., Tunega M., 2013: Nonlinear diffusion filtering of data on the Earth's surface. J. Geod., **87**, 2, 143–160, doi: 10.1007/s00190-012-0587-y.

ESA (European Space Agency), 2014: GOCE Level 2 Product Data Handbook. Issue 5.0, https://earth.esa.int/eogateway/catalog/goce-level-2.

Perona P., Malik J., 1987: Scale space and edge detection using anisotropic diffusion. In: Proceedings of the IEEE Computer Society Workshop on Computer Vision, Miami, FL, 16–27.

Siemes C., 2018: Improving GOCE cross-track gravity gradients. J. Geod., **92**, 1, 33–45, doi: 10.1007/s00190-017-1042-x.